Optics and Photonics Journal, 2022, 12, 64-77
https://www.scirp.org/journal/opj
ISSN Online: 2160-889X
ISSN Print: 2160-8881

Propagation Properties of Multi-Hyperbolic Sine-Correlated Beams in Oceanic Turbulence

Chaoran Hu

College of Science, University of Shanghai for Science and Technology, Shanghai, China
Email: 1197624306@qq.com

How to cite this paper: Hu, C.R. (2022) Propagation Properties of Multi-Hyperbolic Sine-Correlated Beams in Oceanic Turbulence. *Optics and Photonics Journal*, **12**, 64-77.
https://doi.org/10.4236/opj.2022.124005

Received: March 21, 2022
Accepted: April 25, 2022
Published: April 28, 2022

Abstract

As a new partially coherent beam, the propagation properties of the multi-hyperbolic sine-correlated (MHSC) beams in turbulent atmospheres have been studied. But as another important medium, the propagation properties of MHSC beams in oceanic turbulence. This paper has studied these questions in detail. The analytical formulas of spectral density and degree of coherence for the propagation are derived and the numerical simulations are represented. It is found that the intensity patterns of MHSC beams will evolve from dark-hollow profiles into Gaussian profiles caused by oceanic turbulence and will degenerate more rapidly with stronger oceanic turbulence. In addition, the coherence region becomes larger with decreasing in the dissipation rate of turbulence kinetic energy in unit mass liquid or increasing in the relative intensity of temperature and salinity fluctuations, mean square temperature dissipation rate. We also find that the degree of coherence of MHSC beams with a higher-order N will decrease more slowly than those of hyperbolic sine-correlated (HSC) beams.

Keywords

Multi-Hyperbolic Sine-Correlated Beams, Oceanic Turbulence, Spectral Density, Degree of Coherence, Propagate

1. Introduction

Since the sufficient condition to devise genuine spatial correlation functions proposed by Gori and his collaborators [1] opened up a new way for building a spatial correlation function, numerous partially coherent beams with nonconventional correlation functions have been proposed continuously. In the past few years, many new beams have been proposed and their propagation properties have been investigated comprehensively, such as Multi-Gaussian Schell-model beams which can generate far fields with flat intensity profiles [2]; and their behavior of the spectral density and the state of coherence of beamlike fields generated by such sources on propagation in free space and linear isotropic random media are also studied [3]; Twisted Gaussian Schell-model beams which are twisted by a new twist phase about their axis during propagation [4] and their propagation properties in non-Kolmogorov turbulence [5]; lattice-like far field of Twisted Gaussian Schell-model array beams [6] and their propagation properties in anisotropic ocean [7]; the far field of two types of sinc Schell-model beams which carry tunable flat and dark hollow profiles respectively and their propagation characteristics in free space [8]; elliptical ring-shaped beam profile far field of Elliptical Laguerre-Gaussian Schell-model beam [9] and the Statistical properties of a Laguerre-Gaussian Schell-model beam in turbulent atmosphere [10]; shape-invariant ring-shaped intensity distribution of Cosine-Gaussian Schell-model beams [11] and their propagation properties in atmospheric turbulence and non-Kolmogorov turbulence [12]; radially polarized multi-cosine Gaussian Schell-model beams which can generate lattice-like intensity patterns in the focal plane and possess periodic distribution of the degree of polarization [13]; and their propagation properties in non-Kolmogorov turbulence [14]; partially coherent Lorentz-Gauss vortex beams whose transverse pattern in the source plane is the product of two independent Lorentz functions [15] and their propagation properties propagating in a uniaxial crystal orthogonal to the optical axis are studied [16]; Controllable rotating Gaussian Schell-model beams [17]; Partially coherent Pearcey-Gauss beams which maintain the inherent properties of autofocusing performance and inversion effect [18] and Asymmetric twisted vortex Gaussian Schell-model beams which have the form of a crescent rotating upon propagation [19]; Rotating anisotropic Gaussian Schell-model array beams which can generate a field with rotating anisotropic Gaussian array and their propagation properties in free space [20]; Partially coherent elegant Laguerre-Gaussian beams and their coherent vortices properties in the free space [21] and so on. Many studies show that partially coherent beams are less affected by turbulence than fully coherent beams with the consideration of the additional degradation introduced by the turbulence [22] [23]. However, most of the beams possess Schell-model correlations whose correlation function depends on the distance between two spatial points [24]. The far-field intensity distribution of such fields is proportional to the Fourier transform of the source correlation function [25]. So the distribution of the radiant intensity is independent of the shape of the source. Recently, Mei proposed a new beam called hyperbolic sine-correlated beam (HSC) with non-Schell-model correlations whose profile of spectral density presents a dark-hollow shape and remains invariant from the source field to the far-field [26]. The propagation properties of hyperbolic sine correlated beams in free space are also studied. Then, Song proposed multi-hyperbolic sine-correlated beams (MHSC) on the basis of Mei and studied the propagation properties of MHSC beams in a turbulent atmosphere [27]. But in other media like oceanic turbulence, the propagation characteristic of MHSC beams has been investigated.

As a novel kind of random medium, oceanic turbulence has a great influence on the propagation properties of random beams. With the development of underwater optical communication, imaging, remote sensing, and other fields [28] [29] [30] [31] [32], the propagation of random beams in oceanic turbulence attracted more and more researchers. Some significant models are established [33] as a novel kind of media, unlike turbulent atmosphere, oceanic turbulence exerts influence on the propagation properties of random beams by both temperature and salinity fluctuation. Two kinds of fluctuation have been researched respectively for a long time until an analytical model for a spatial power spectrum combining both salinity and temperature fluctuation has been proposed [34]. There may be a big difference between the propagation properties in oceanic turbulence and other media or free space. It's very interesting for researchers to investigate what types of light beams and under what conditions oceanic turbulence has the smallest influence. It is necessary to investigate how MHSC beams propagate in oceanic turbulence and their propagation properties including spectral density and degree of coherence.

In this paper, an analytical model for a spatial power spectrum combining both salinity and temperature fluctuation is taken into consideration [34]. We compare the spectral intensity distribution of MHSC beams in free space and oceanic turbulence. The spectral intensity distribution can keep the dark-hollow profile invariant propagating in free space. However, in oceanic turbulence, the dark-hollow profile will be gradually destroyed after propagating a certain distance. Then we focus on the changes in the spectral density and the degree of coherence (DOC) of MHSC beams propagating in the clear-water turbulent ocean. To illustrate this, some analytical formulae will be derived and numerical calculations will be presented. Some interesting and useful results will also be discussed. This paper also provides potential applications in underwater optical communication, imaging, and remote sensing by multi-hyperbolic sine-correlated beams.

2. Theoretic Analysis of the Propagation of MHSC Beams in Oceanic Turbulence

We consider a statistically stationary partially coherent scalar beam propagating from the source plane $z = 0$ into the positive half-space $z > 0$ in the space-frequency domain. For brevity, the analysis of the field is limited to one transverse dimension x, but the generalization of the results to a two-dimensional (2D) case is straightforward. Supposing x_1' and x_2' are the position coordinate of two points in the initial plane, the second-order correlation properties of the field can be characterized by the cross-spectral density (CSD) function $W_0\left(x_1', x_2'\right)$. The $W_0\left(x_1', x_2'\right)$ is a sufficient nonnegative definiteness, which can be expressed as a superposition integral of the form [1]:

$$W_0\left(x_1', x_2'\right)=\int p(v) H^*\left(x_1', v\right) H\left(x_2', v\right) \mathrm{d} v \tag{1}$$

here $p(v)$ is an arbitrary nonnegative weight function, H is an arbitrary integral kernel and the asterisk represents a complex conjugate that defines the correlation class of a light field. For brevity, the dependence on the frequency is ignored.

For generating a light source whose spectral intensity presents a dark-hollow shape and remains invariant from the source field to the far-field, a kernel H of Fourier-sine form was considered by Mei as [26],

$$H\left(x', v\right)=\exp\left(-\frac{x'^2}{\sigma^2}\right) \sin\left(x' v\right), \tag{2}$$

and the weight function with Gaussian distribution is set as [26] [27].

$$p(v)=\frac{\delta}{2\sqrt{\pi} C} \sum_{n=1}^N\binom{N}{n} \frac{(-1)^{n-1}}{\sqrt{n}} \exp\left(-\frac{n \delta^2 v^2}{4}\right), \tag{3}$$

where $C=\sum_{n=1}^N\binom{N}{n} \frac{(-1)^{n-1}}{n}$ is the normalized factor, $\binom{N}{n}$ is binomial coefficients.

Substituting Equations (2) and (3) into Equation (1), the cross-spectral density function (CSDF) of any MHSC beams at the initial plane can be derived as [27].

$$W_0\left(x_1', x_2'\right)=\frac{1}{C} \sum_{n=1}^N\binom{N}{n} \frac{(-1)^{n-1}}{n} \times \exp\left(-\frac{x_1'^2+x_2'^2}{\omega_n^2}\right) \sinh\left(\frac{2 x_1' x_2'}{n \delta^2}\right), \tag{4}$$

where $\omega_n^{-2}=\sigma^{-2}+n^{-1} \delta^{-2}$, parameter δ represents the spatial coherence length, parameter ω_n represents the beam width and parameter σ is positive real constant.

When an MHSC beam propagates through oceanic turbulence, the cross-spectral density function of any two points on the output plane can be obtained by the following extended Huygens-Fresnel principle [35],

$$\begin{aligned} W\left(x_1, x_2, z\right)= & \frac{k}{2 \pi z} \iint W_0\left(x_1', x_2'\right) \times \exp\left[-\frac{i k}{2 z}\left(x_1-x_2'\right)^2+\frac{i k}{2 z}\left(x_2-x_2'\right)^2\right] \\ & \times\left\langle\exp\left[\psi^*\left(x_1, x_1', z\right)+\psi^*\left(x_2, x_2', z\right)\right]\right\rangle_m \mathrm{d} x_1' \mathrm{d} x_2', \end{aligned} \tag{5}$$

among [34].

$$\begin{aligned} & \left\langle\exp\left[\psi^*\left(x_1, x_1', z\right)+\psi\left(x_2, x_2', z\right)\right]\right\rangle_m \\ & \cong \exp\left\{-\frac{k^2 z T}{3}\left[\left(x_1-x_2\right)^2+\left(x_1-x_2\right) \times\left(x_1'-x_2'\right)+\left(x_1'-x_2'\right)^2\right]\right\} \mathrm{d} x_1' \mathrm{d} x_2', \end{aligned} \tag{6}$$

with

$$T=\pi^2 \int_0^{\infty} \kappa^3 \Phi_n(\kappa) \mathrm{d} \kappa, \tag{7}$$

where T represents the intensity of the turbulence, $\Phi_n(\kappa)$ is the one-dimensional power spectrum of fluctuations in the refractive index of the random medium and κ is the spatial frequency.

To simulate the oceanic turbulence, we use the spatial power spectrum $\Phi_n(\kappa)$ where combined effects of temperature and salinity fluctuations are considered as [36].

$$\Phi_n(\kappa) = 0.388 \times 10^{-8} \varepsilon^{-1/3} \kappa^{-11/3} \left[1 + 2.35(\kappa\eta)^{2/3}\right] f(\kappa, w, \chi_T), \tag{8}$$

with

$$f(\kappa, \omega, \chi_T) = \chi_T \left(e^{-A_T\delta} + w^{-2} e^{-A_S\delta} - 2w^{-1} e^{-A_{TS}\delta}\right), \tag{9}$$

where ε is the rate of dissipation of turbulent kinetic energy per unit mass of fluid, which may vary in range from 10^{-10} m²/s³ to 10^{-1} m²/s³, $\eta = 10^{-3}$ m is the Kolmogorov micro-scale (inner scale), χ_T stands for the rate of dissipation of mean-square temperature ranging from 10^{-10} K²/s to 10^{-4} K²/s, $A_T = 1.863 \times 10^{-2}$, $A_S = 1.9 \times 10^{-4}$, + $A_{TS} = 9.41 \times 10^{-3}$, $\delta = 8.284(\kappa\eta)^{4/3} + 12.978(\kappa\eta)^2$, w (non-dimensional) represents the relative strength of temperature and salinity fluctuations, which can vary in the interval [−5, 0], $w = -5$ corresponds to the dominating temperature-induced optical turbulence while $w = 0$ corresponds to that induced by salinity.

Through numerical integral, Equation (7) can be expressed as:

$$\begin{aligned} T = \pi^2 \Big[& 0.388 \times 10^{-8} \varepsilon^{-1/3} \eta^{-1/3} \chi_T \\ & \times \left(47.5708 w^{-2} - 17.6701 w^{-1} + 6.78335\right)\Big]. \end{aligned} \tag{10}$$

On substituting Equations (6) and (10) into Equation (5), one can obtain the expression of CSD of MHSC at any plane as:

$$\begin{aligned} W(x_1, x_2, z) = {} & \frac{k}{4zC} \exp\left[\frac{ik}{2z}\left(x_1^2 - x_2^2\right)\right] \exp\left[-\frac{k^2 zT}{3}(x_1 - x_2)^2\right] \\ & \times \sum_{n=1}^{N} \binom{N}{n} \frac{(-1)^{n-1}}{n} \frac{1}{\sqrt{a}} \exp\left(\frac{d_1^2}{4a}\right) \left\{ \frac{1}{\sqrt{c_1}} \exp\left[\frac{(d_2 - b_1 d_1/a)}{4c_1}\right] \right. \\ & \left. - \frac{1}{\sqrt{c_2}} \exp\left[\frac{(d_2 - b_2 d_1/a)}{4c_2}\right] \right\}, \end{aligned} \tag{11}$$

with

$$a = \frac{1}{\omega_n^2} - \frac{ik}{2z} + \frac{k^2 zT}{3}, b_1 = \frac{1}{n\delta^2} + \frac{k^2 zT}{3}, b_2 = -\frac{1}{n\delta^2} + \frac{k^2 zT}{3};$$

$$c_1 = \frac{1}{\omega_n^2} + \frac{ik}{2z} + \frac{k^2 zT}{3} - \frac{b_1^2}{a}, c_2 = \frac{1}{\omega_n^2} + \frac{ik}{2z} + \frac{k^2 zT}{3} - \frac{b_2^2}{a};$$

$$d_1 = \frac{ikx_1}{z} + \frac{k^2 zT}{3}(x_1 - x_2), d_2 = \frac{ikx_2}{z} + \frac{k^2 zT}{3}(x_1 - x_2).$$

We let $x_1 = x_2 = x$ and the spectral density of the MHSC beams $S(x, z)$ is equivalent to the CSDF $W(x, x, z)$. The spectral intensity of the MHSC beam in the oceanic turbulence can be derived as:

$$\begin{aligned}
&S(x,z)=W(x,x,z)\\
&=\frac{k}{4zC}\sum_{n=1}^{N}\binom{N}{n}\frac{(-1)^{n-1}}{n}\frac{1}{\sqrt{a}}\exp\left(-\frac{k^2x^2}{4az^2}\right)\\
&\times\left\{\frac{1}{\sqrt{c_1}}\exp\left[-\frac{k^2x^2(1-b_1/a)^2}{4c_1z^2}\right]-\frac{1}{\sqrt{c_2}}\exp\left[-\frac{k^2x^2(1-b_2/a)^2}{4c_2z^2}\right]\right\},
\end{aligned} \tag{12}$$

the degree of coherence (DOC) which can be used to describe the associated degree of two arbitrary points in the propagation plane can be derived as [25].

$$\mu(x_1,x_2,z)=\frac{W(x_1,x_2,z)}{\sqrt{W(x_1,x_1,z)W(x_2,x_2,z)}}. \tag{13}$$

In this paper, we set $\sigma=0.05\ \text{m}$, $\delta=0.02\ \text{m}$, $N=5$ which represents the number of contours of beams, $\lambda=632.8\ \text{nm}$ which represents wavelength, $\chi_T=10^{-7}\ \text{K}^2/\text{s}$, $\varepsilon=10^{-5}\ \text{m}^2/\text{s}^3$, $w=-2.5$ unless other parameters values are set.

Figure 1 shows the evolution of spectral density on the *x-z* plane and the lateral distribution of the MHSC beam at several selected distances in free space and oceanic turbulence on propagation. In free space, the spectral density distribution of the MHSC beam remains a dark-hollow pattern invariant during the propagating process and the beam will spread as the propagation distance increases. According to the side view, there are two intensity peaks at symmetrical positions on both sides of the origin. With the increasing of propagation distance, the values of two peaks will decrease and the size of the central dark spot will

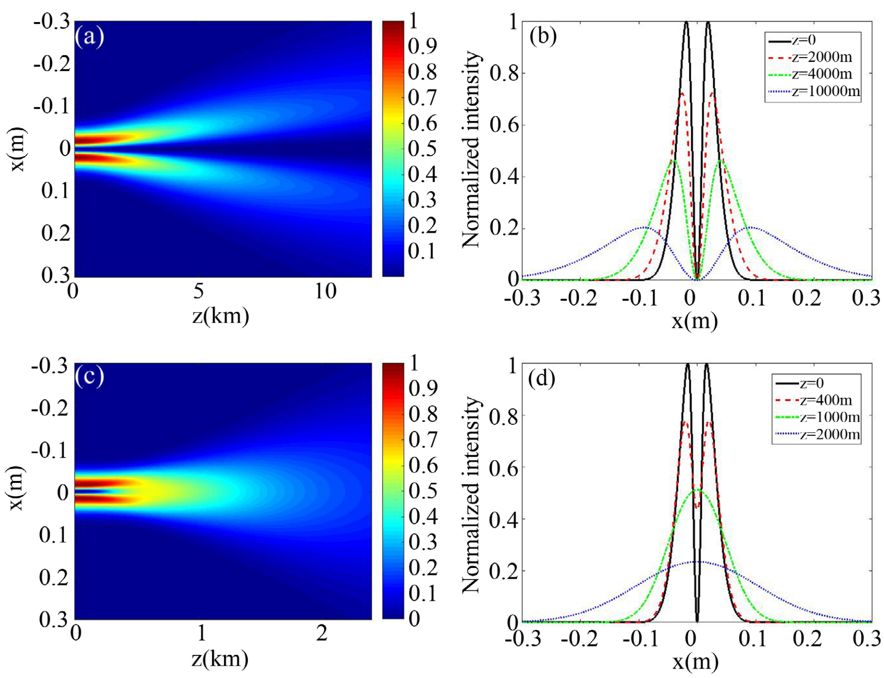

Figure 1. The evolution of spectral density on the *x-z* plane and the lateral distribution for several selected propagation distances of the MHSC beam in (a)-(b) free space and (c)-(d) oceanic turbulence.

expand. While in the oceanic turbulence, after propagating through a certain distance, the dark-hollow spectral density profile will converge into a Gaussian-like shape gradually. And the spread rate of the beams is faster than that in free space. In addition, different from the free-space propagation, the central intensity increases with the decline of two peaks through oceanic propagation, until the whole distribution completely evolves into a Gaussian-like shape. The propagation behavior can be explained by the combined effects of source correlation and oceanic turbulence. In the near field, the source correlation dominates the evolution of spectral density. Therefore, the near-field spectral density keeps a dark-hollow profile in both free space and oceanic turbulence. But in the far-field, the growing influence of oceanic turbulence will finally result in Gaussian intensity distribution.

3. Numerical Simulation and Analysis of Spectral Density of the MHSC Beams in an Oceanic Turbulence

In this section, we will investigate the spectral density of the MHSC beams. Then the numerical simulations and analyses of the $S(x,z)$ are presented.

Figure 2 shows the influence of parameter *N* on the spectral density of MHSC beams propagating in oceanic turbulence. In the near field, there are two peaks of spectral density at symmetrical positions on both sides of the origin and the spectral density presents a dark-hollow shape. With a larger *N*, the area of the dark spot is a little smaller, which means the spread rate of the beams slightly slows down. In the far-field, the spectral density distribution evolves into a Gaussian shape, and the decline rate of spectral density around the origin becomes faster with the increase of *N*.

Figure 3 shows how the parameter χ_T affects the spectral density of MHSC beams on propagation in oceanic turbulence. In the near-field, when χ_T is very small, the spectral density presents a dark-hollow shape. There are two peaks at symmetrical positions on both sides of the origin. When χ_T grows, the two peaks of spectral density decrease, the spectral density at the origin increases. The pattern of spectral density distribution evolves from a dark-hollow shape

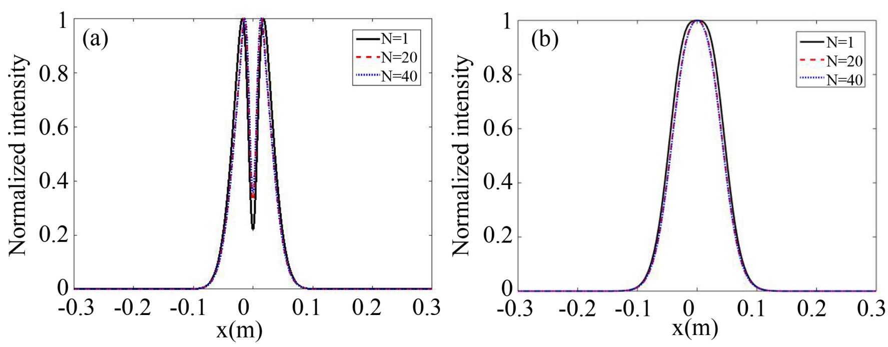

Figure 2. The spectral density (a)-(b) of MHSC beams propagating in oceanic turbulence varies with the parameter N at different distances, $\chi_T = 10^{-7}\,\mathrm{K}^2/\mathrm{s}$, $\varepsilon = 10^{-5}\,\mathrm{m}^2/\mathrm{s}^3$, $w = -2.5$, (a) $z = 200$ m, (b) $z = 1000$ m.

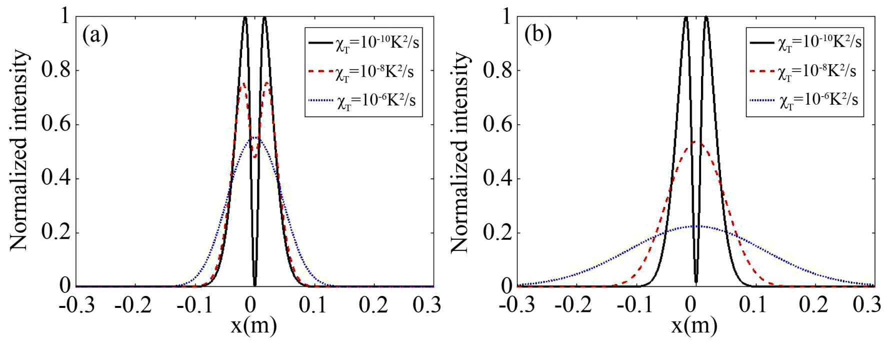

Figure 3. The spectral density (a)-(b) of MHSC beams propagating in oceanic turbulence varies with the parameter χ_T at different distances, $N = 5$, $\varepsilon = 10^{-5}\,\mathrm{m}^2/\mathrm{s}^3$, $w = -2.5$, (a) $z = 200$ m, (b) $z = 1000$ m.

into a Gaussian shape and the MHSC beams spread. In the far-field, as χ_T becomes larger, the spectral density distribution evolves from a dark-hollow shape to a Gaussian shape and the beams spread. The spread rate of the beams is faster than in the near-field.

Figure 4 shows how the parameter ε has an effect on the spectral density of MHSC beams' behavior propagating in oceanic turbulence. In the near field, the spectral density is a Gaussian shape with a tiny ε. As ε increases, the spectral density at the origin declines. There are two peaks at symmetrical positions on both sides of the origin. The spectral density will turn into a dark-hollow shape. In the far field, when ε is very small, the spectral density distribution takes on a Gaussian shape. With the growth of ε, the peak of spectral density increases, and the spot size is smaller.

Figure 5 shows the spectral density of MHSC beams propagating in oceanic turbulence changes with the parameter w. In the near field, when the value of w is relatively small, the spectral density at the origin is also small and there are two peaks at symmetrical positions on both sides of the origin. As w grows, the two peaks of spectral density decline, and the spectral density at the origin increases. The beams hardly spread. In the far-field, as w increases, the spectral density evolves from a dark hollow shape to a Gaussian shape and the beams spread. The speed of evolution is faster than in the near-field.

4. Numerical Simulation and Analysis of Degree of Coherence of the MHSC Beams in an Oceanic Turbulence

We always use the degree of coherence to describe the associated degree of two points in the field. In this section, we set $x_2 = 0$. The DOC of the MHSC beams thus can be expressed as:

$$\mu(x_1,0,z) = \frac{W(x_1,0,z)}{\sqrt{W(x_1,x_1,z)W(0,0,z)}} \tag{14}$$

Figure 6 shows how the parameter N influences DOC of MHSC beams propagating in oceanic turbulence. In the near field, the degree of coherence has

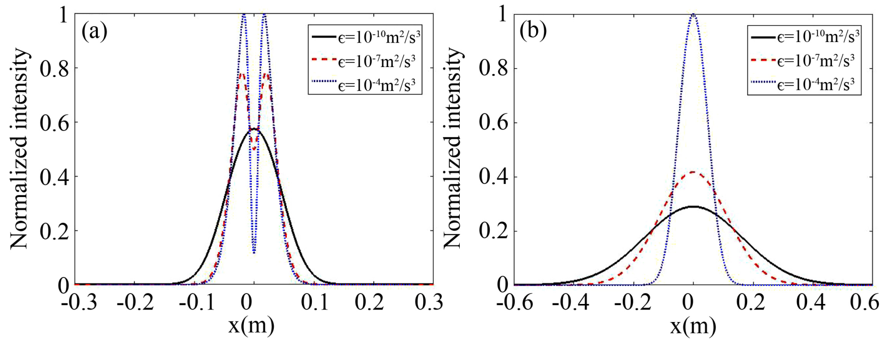

Figure 4. The spectral density of MHSC beam propagating in oceanic turbulence varies with the parameter ε at different distances, $N = 5$, $\chi_T = 10^{-7}\ \mathrm{K}^2/\mathrm{s}$, $w = -2.5$, (a) $z =$ 200 m, (b) $z = 1000$ m.

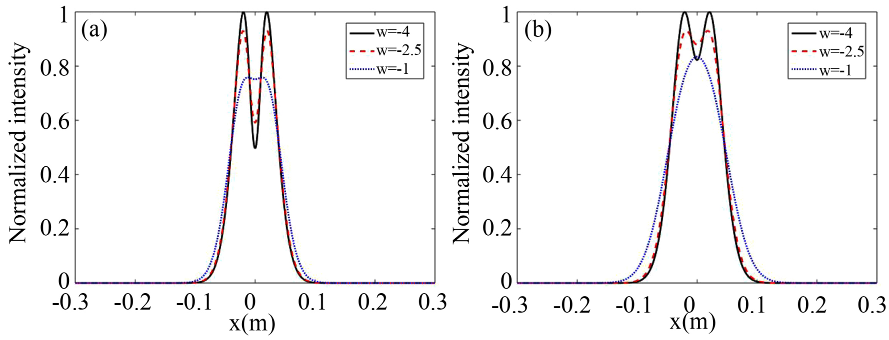

Figure 5. The spectral density of MHSC beam propagating in oceanic turbulence varies with the parameter w at different distances, $N = 5$, $\chi_T = 10^{-7}\ \mathrm{K}^2/\mathrm{s}$, $\varepsilon = 10^{-7}\ \mathrm{m}^2/\mathrm{s}^3$, (a) $z =$ 200 m, (b) $z = 1000$ m.

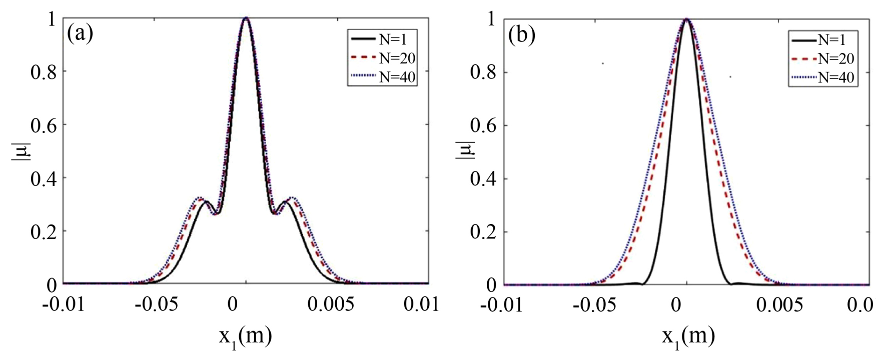

Figure 6. The degree of coherence (DOC) of MHSC beams propagating in oceanic turbulence varies with the parameter N at different distances, $\chi_T = 10^{-7}\ \mathrm{K}^2/\mathrm{s}$, $\varepsilon = 10^{-5}\ \mathrm{m}^2/\mathrm{s}^3$, $w = -2.5$, (a) $z = 200$ m, (b) $z = 1000$ m.

three maxima. In addition to a main peak at the origin, there are also two secondary peaks at symmetrical positions on both sides of the origin. When the parameter N increases, the coherence region will become larger. In the far-field, the distribution of coherence is a Gaussian shape. The decline rate of DOC is slower which means the coherence region becomes larger with the growth of parameter N.

Figure 7 shows the influence of DOC on MHSC beams propagating in oceanic turbulence. In the near field, the degree of coherence has three maximum values. In addition to the main peak at the origin, there are also two secondary peaks at symmetrical positions on both sides of the origin. When χ_T increases, the positions where the two secondary peaks appear are closer to the origin. The coherence region reduces and the two secondary peaks decrease. In the far-field, when χ_T is small, the DOC has three peaks and the two secondary peaks are far away from the origin. The coherence region is relatively large. When χ_T grows, the coherence region decreases, and the two secondary peaks disappear. The DOC evolves into a Gaussian shape.

Figure 8 shows how DOC of MHSC beams propagating in oceanic turbulence changes with the parameter ε. In the near-field, the degree of coherence has three maxima. In addition to the main peak at the origin, there are also two secondary peaks at symmetrical positions on both sides of the origin; when ε is very small, the positions where two secondary peaks appear are close to the origin, the coherence region is relatively small and the two secondary peaks are also small. When ε increases, the positions where the secondary peaks appear are far away from the origin. The coherence region becomes larger, and the secondary

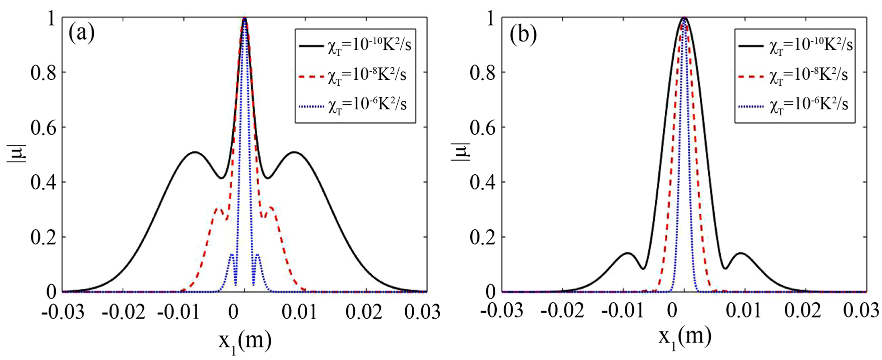

Figure 7. The degree of coherence (DOC) of MHSC beams propagating in oceanic turbulence varies with the parameter χ_T at different distances, $N = 5$, $\varepsilon = 10^{-5}\ \mathrm{m^2/s^3}$, $w = -2.5$, (a) $z = 200$ m, (b) $z = 1000$ m.

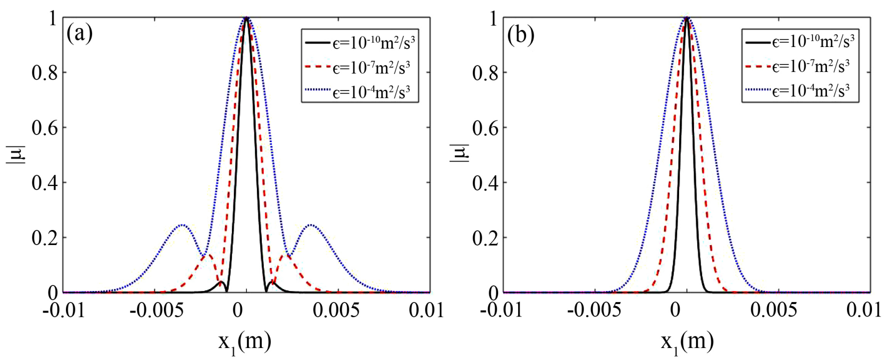

Figure 8. The DOC of MHSC beam propagating in oceanic turbulence varies with the parameter ε at different distances, $N = 5$, $\chi_T = 10^{-7}\ \mathrm{K^2/s}$, $w = -2.5$, (a) $z = 200$ m, (b) $z = 1000$ m.

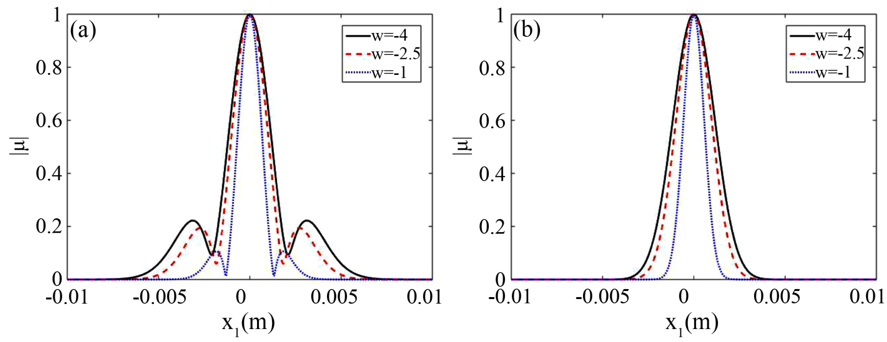

Figure 9. The DOC of MHSC beam propagating in oceanic turbulence varies with the parameter w at different distances, $N = 5$, $\chi_T = 10^{-7}\,\mathrm{K^2/s}$, $\varepsilon = 10^{-7}\,\mathrm{m^2/s^3}$, (a) $z = 200$ m, (b) $z = 1000$ m.

peaks corresponding to the DOC become larger. In the far-field, the distribution of coherence is Gaussian shape. The coherence region is small when ε is very small and becomes larger with the increase of ε.

Figure 9 shows how the parameter w affects DOC of MHSC beams propagating in oceanic turbulence. In the near field, there are two secondary peaks at symmetrical positions on both sides of the origin except the main peak. As w is small, the secondary peaks appear farther from the origin and the coherence region is relatively large. When w increases, the positions where the two secondary peaks appear become closer to the origin. The coherence region decreases and the two secondary peaks become smaller. In the far-field, the distribution of coherence is Gaussian shape. When w is small, the DOC reduces slowly and the coherence region is large. With the growth of w, the DOC decreases faster and the coherence region reduces.

5. Discussion

For a long time, unlike a large number of literatures about laser turbulent propagation in the atmosphere, ocean turbulence has received less attention due to its complexity. Oceanic turbulence has an influence on the propagation properties of random beams by both temperature and salinity fluctuation. Two kinds of fluctuation have been researched respectively for a long time until an analytical model for a spatial power spectrum combining both salinity and temperature fluctuation has been proposed. This model can better simulate some characteristics of realistic ocean turbulence with the consideration of both two factors.

6. Conclusion

In summary, we first derive the general expression for the CSDF of MHSC beams propagating through oceanic turbulence on the basis of the extended Huygens–Fresnel principle. Then the expressions of spectral density and degree of coherence (DOC) are easily obtained. Unlike the dark-hollow shape in free space and the flat-topped profile in a turbulent atmosphere [27], our numerical simulation shows that the distribution of spectral density will evolve from a dark-hollow shape into a Gaussian-like profile and the distribution of DOC will converge from a three peaks shape into a Gaussian-like profile through the propagation in the oceanic turbulence. During the propagation process, the beams are influenced by both the light source and the oceanic turbulence. In a short propagation distance, the light source dominates the distribution of spectral density and DOC of MHSC beams. When the MHSC beams propagate into a relatively far distance, oceanic turbulence has a great influence. The beams will spread more slowly and the coherence region would decrease more slightly with the increase of the dissipation rate of turbulence kinetic energy in unit mass liquid or the decrease of the relative intensity of temperature and salinity fluctuations, mean square temperature dissipation rate. Our study will be helpful for the operation of communication, imaging, and sensing systems involving turbulent underwater channels.

Conflicts of Interest

The author declares no conflicts of interest regarding the publication of this paper.

References

[1] Gori, F. and Santarsiero, M. (2007) Devising Genuine Spatial Correlation Functions. *Optics Letters*, **32**, 3531-3533. https://doi.org/10.1364/OL.32.003531

[2] Sahin, S. and Korotkova, O. (2012) Light Sources Generating Far Fields with Tunable Flat Profiles. *Optics Letters*, **37**, 2970-2972. https://doi.org/10.1364/OL.37.002970

[3] Korotkova, O., Sahin, S. and Shchepakina, E. (2012) Multi-Gaussian Schell-Model Beams. *Journal of the Optical Society of America A—Optics Image Science and Vision*, **29**, 2159-2164. https://doi.org/10.1364/JOSAA.29.002159

[4] Simon, R. and Mukunda, N. (1993) Twisted Gaussian Schell-Model Beams. *Journal of the Optical Society of America A* (*Optics and Image Science*), **10**, 95-109. https://doi.org/10.1364/JOSAA.10.000095

[5] Cui, Y., Wang, F. and Cai, Y.J. (2014) Propagation of a Twist Gaussian-Schell Model Beam in Non-Kolmogorov Turbulence. *Optics Communications*, **324**, 108-113. https://doi.org/10.1016/j.optcom.2014.03.030

[6] Wan, L.P. and Zhao, D.M. (2018) Twisted Gaussian Schell-Model Array Beams. *Optics Letters*, **43**, 3554-3557. https://doi.org/10.1364/OL.43.003554

[7] Tang, M.M. and Li, H.H. (2020) Statistical Properties of Twisted Gaussian Schell-Model Array Beams in Anisotropic Ocean. *Optik*, **211**, Article ID: 164612. https://doi.org/10.1016/j.ijleo.2020.164612

[8] Mei, Z.R. (2014) Two Types of Sinc Schell-Model Beams and Their Propagation Characteristics. *Optics Letters*, **39**, 4188-4191. https://doi.org/10.1364/OL.39.004188

[9] Chen, Y.H., Liu, L., Wang, F., Zhao, C.L. and Cai, Y.J. (2014) Elliptical Laguerre-Gaussian Correlated Schell-Model Beam. *Optics Express*, **22**, 13975-13987. https://doi.org/10.1364/OE.22.013975

[10] Chen, R., Liu, L., Zhu, S.J., Wu, G.F., Wang, F. and Cai, Y.J. (2014) Statistical Properties of a Laguerre-Gaussian Schell-Model Beam in Turbulent Atmosphere. *Optics Express*, **22**, 1871-1883. https://doi.org/10.1364/OE.22.001871

[11] Mei, Z.R. and Korotkova, O. (2013) Cosine-Gaussian Schell-Model Sources. *Optics Letters*, **38**, 2578-2580. https://doi.org/10.1364/OL.38.002578

[12] Xu, H.F., Zhang, Z., Qu, J. and Huang, W. (2014) Propagation Factors of Cosine-Gaussian-Correlated Schell-Model Beams in Non-Kolmogorov Turbulence. *Optics Express*, **22**, 22479-22489. https://doi.org/10.1364/OE.22.022479

[13] Tang, M.M., Zhao, D.M., Li, X.Z. and Li, H.H. (2017) Focusing Properties of Radially Polarized Multi-Cosine Gaussian Correlated Schell-Model Beams. *Optics Communications*, **396**, 249-256. https://doi.org/10.1016/j.optcom.2017.03.063

[14] Tang, M.M., Zhao, D.M., Li, X.Z. and Wang, J.G. (2018) Propagation of Radially Polarized Multi-Cosine Gaussian Schell-Model Beams in Non-Kolmogorov Turbulence. *Optics Communications*, **407**, 392-397. https://doi.org/10.1016/j.optcom.2017.09.067

[15] El Gawhary, O. and Severini, S. (2006) Lorentz Beams and Symmetry Properties in Paraxial Optics. *Journal of Optics A—Pure and Applied Optics*, **8**, 409-414. https://doi.org/10.1088/1464-4258/8/5/007

[16] Liu, D.J., Zhong, H.Y., Wang, G.Q., Yin, H.M. and Wang, Y.C. (2019) Evolution Properties of a Partially Coherent Lorentz-Gauss Vortex Beam in a Uniaxial Crystal. *Journal of Modern Optics*, **66**, 67-76. https://doi.org/10.1080/09500340.2018.1511865

[17] Wan, L.P. and Zhao, D.M. (2019) Controllable Rotating Gaussian Schell-Model Beams. *Optics Letters*, **44**, 735-738. https://doi.org/10.1364/OL.44.000735

[18] Zhou, X.Y., Pang, Z.H. and Zhao, D.M. (2020) Partially Coherent Pearcey-Gauss Beams. *Optics Letters*, **45**, 5496-5499. https://doi.org/10.1364/OL.404277

[19] Zhang, Y., Pan, K.M., Xu, J., Zhu, W.T. and Zhao, D.M. (2021) Asymmetric Twisted Vortex Gaussian Schell-Model Beams. *Optics Communications*, **491**, Article ID: 126950. https://doi.org/10.1016/j.optcom.2021.126950

[20] Zheng, S.M., Huang, J., Ji, X.L., Cheng, K. and Wang, T. (2021) Rotating Anisotropic Gaussian Schell-Model Array Beams. *Optics Communications*, **484**, Article ID: 126684. https://doi.org/10.1016/j.optcom.2020.126684

[21] Dong, M. and Yang, Y. (2020) Coherent Vortices Properties of Partially Coherent Elegant Laguerre-Gaussian Beams in the Free Space. *Optics and Photonics Journal*, **10**, 159-166. https://doi.org/10.4236/opj.2020.106017

[22] Santarsiero, M., Gori, F., Borghi, R., Cincotti, G. and Vahimaa, P. (1999) Spreading Properties of Beams Radiated by Partially Coherent Schell-Model Sources. *Journal of the Optical Society of America A*: *Optics & Image Science*, **16**, 106-112. https://doi.org/10.1364/JOSAA.16.000106

[23] Shirai, T., Dogariu, A. and Wolf, E. (2003) Mode Analysis of Spreading of Partially Coherent Beams Propagating through Atmospheric Turbulence. *Journal of the Optical Society of America A*, **20**, 1094-1102. https://doi.org/10.1364/JOSAA.20.001094

[24] Mandel, L., Wolf, E. and Shapiro, J.H. (1996) Optical Coherence and Quantum Optics. *Physics Today*, **49**, 68-70. https://doi.org/10.1063/1.2807623

[25] Wolf, E. and Meystre, P. (2008) Introduction to the Theory of Coherence and Polarization of Light. *Physics Today*, **61**, 59-60.

[26] Mei, Z.R. (2019) Hyperbolic Sine-Correlated Beams. *Optics Express*, **27**, 7491-7497. https://doi.org/10.1364/OE.27.007491

[27] Song, Z.Z., Zhao, D.Y., Han, Z.Y., Ye, J.F., Wang, J.F., Sun, T.T., Liu, Z.J., Liu, S.T. and Liu, B. (2020) Multi-Hyperbolic Sine-Correlated Beams and Their Statistical Prop-

erties in Turbulent Atmosphere. *Journal of the Optical Society of America A—Optics Image Science and Vision*, **37**, 1595-1602. https://doi.org/10.1364/JOSAA.397872

[28] Arnon, S. (2010) Underwater Optical Wireless Communication Network. *Optical Engineering*, **49**, Article ID: 015001. https://doi.org/10.1117/1.3280288

[29] Hou, W.L. (2009) A Simple Underwater Imaging Model. *Optics Letters*, **34**, 2688-2690. https://doi.org/10.1364/OL.34.002688

[30] Hou, W.L., Jarosz, E., Woods, S., Goode, W. and Weidemann, A. (2013) Impacts of Underwater Turbulence on Acoustical and Optical Signals and Their Linkage. *Optics Express*, **21**, 4367-4375. https://doi.org/10.1364/OE.21.004367

[31] Hou, W.L., Woods, S., Jarosz, E., Goode, W. and Weidemann, A. (2012) Optical Turbulence on Underwater Image Degradation in Natural Environments. *Applied Optics*, **51**, 2678-2686. https://doi.org/10.1364/AO.51.002678

[32] Johnson, L.J., Green, R.J. and Leeson, M.S. (2014) Underwater Optical Wireless Communications: Depth-Dependent Beam Refraction. *Applied Optics*, **53**, 7273-7277. https://doi.org/10.1364/AO.53.007273

[33] Liu, Y., Zeng, C. and Luo, Y. (2018) Dynamics of a New Rumor Propagation Model with the Spread of Truth. *Applied Mathematics*, **9**, 536-549. https://doi.org/10.4236/am.2018.95038

[34] Nikishov, V.V. and Nikishov, V.I. (2000) Spectrum of Turbulent Fluctuations of the Sea-Water Refraction Index. *International Journal of Fluid Mechanics Research*, **27**, 82-98. https://doi.org/10.1615/InterJFluidMechRes.v27.i1.70

[35] Shirai, T., Dogariu, A. and Wolf, E. (2003) Mode Analysis of Spreading of Partially Coherent Beams Propagating through Atmospheric Turbulence. *Journal of the Optical Society of America A—Optics Image Science and Vision*, **20**, 1094-1102. https://doi.org/10.1364/JOSAA.20.001094

[36] Toselli, I., Andrews, L.C., Phillips, R.L. and Ferrero, V. (2008) Free-Space Optical System Performance for Laser Beam Propagation through Non-Kolmogorov Turbulence. *Optical Engineering*, **47**, Article ID: 026003. https://doi.org/10.1117/1.2870113